JISSE
ISSN: 2636-4425

Journal of International Society for Science and Engineering
Vol. 3, No. 3, 46-52 (2021)

JISSE
E-ISSN:2682-3438

Identification and Analysis of Servo-Pneumatic System using Mixed Reality Environment

Magdy Awad[1,*], Saber A. Rabbo[2], Mohamed El-Arabi[3]

[1] *Mechatronics Engineering Department, Canadian International College, 5Th Settlement, Cairo 11835, Egypt*

[2] *Department of Mechanical Engineering, Faculty of Engineering at Shoubra, Benha University, Egypt.*

[3] *Department of Design and Production Engineering, Faculty of Engineering, Cairo University, Giza 12613, Egypt*

ARTICLE INFO

Article history:
Received: 02/07/2021
Accepted: 2021-09-01
Online: 2021-09-01

Keywords:
Online system identification.
Mixed-reality environment
Auto-regressive moving-average
Servo pneumatic system

ABSTRACT

This paper presents a method to control and identify the servo pneumatic system using a mixed reality environment. A mathematical model is presented to study the system dynamics and nonlinear effects of the servo pneumatic system. The auto-regressive moving-average (ARMA) model-based recursive least squares (RLS) algorithm is utilized to identify the transfer function of the servo pneumatic system in a real-time environment. The identification of the servo pneumatic system can be carried out effectively and efficiently using the proposed ARMA model. Furthermore, the high precision to identify the system with minimum error, and reducing the time in adjusting the parameters of the control unit. The discrete transfer function of the servo pneumatic system is identified in real-time from the inputs and outputs data of the system. The identification results showed that the fourth-order system model achieved the minimum square error with one-step prediction. The experimental results showed the accuracy and effectiveness of the proposed method.

1. Introduction

Servo pneumatic systems present an alternative to electric motors and hydraulic systems for industrial applications. Pneumatic systems are generally clean, robust, and reliable in operation. Moore and Pu provided an overview of the growth of servo pneumatic systems technologies [1]. Servo pneumatic systems are considered non-linear systems due to air compressibility, external forces, disturbances, and leakage. Moreover, it is difficult to accurately represent the performance of servo pneumatic systems. Therefore, linear models about the operating points of the non-linear servo pneumatic systems have been presented in [2-5]. The motion control of servo-pneumatic systems has been improved in a lot of previous studies via different advanced control techniques [6-9]. PID controller is widely used in servo pneumatic positioning systems. Recent studies have dealt with different control methods for precise pneumatic positioning in real-time such as PID-based controller [10-15], fuzzy control [16, 17]. Kamaludin, et al. investigated the stability of a PI controller in a servo pneumatic positioning application [18]. In this paper, a method to identify and control electro-pneumatic servo drives in a real-time environment is presented. The Auto-regressive moving-average (ARMA) model is employed to identify the transfer function of the system. PID controller gains are optimized and applied to the simulated model and experimental system.

2. System Description and non-linear mathematical model

The pneumatic system consists of an electro-pneumatic servo drive and pneumatic cylinder subjected to the load. Figure 1 illustrates diagrammatically the relationship of the cylinder's chambers and the inlet connections.

2.1 Modeling of pneumatic valve and actuator

Development of a model for a pneumatic valve and actuator requires mathematical relations for the mass flow rate through the valve, the pressure, volume, and temperature of the air in cylinder chambers, and the actuator load dynamics. A typical arrangement of a five-port valve used to control an actuator is shown in Figure 2. The actuator is positioned horizontally so gravity effects can be ignored.

*Magdy Awad, Mechatronics Engineering Department, Canadian International College, Cairo, Egypt, +201229853338, magdy_n_ibrahim@cic-cairo.com

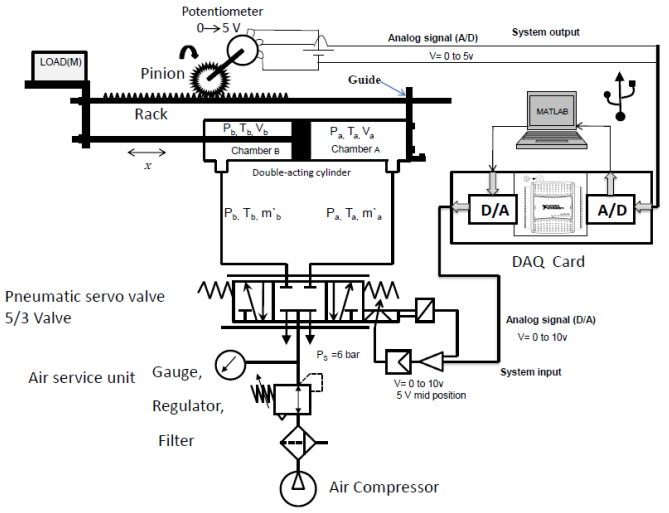

Figure 1: Schematic diagram of the pneumatic experimental system.

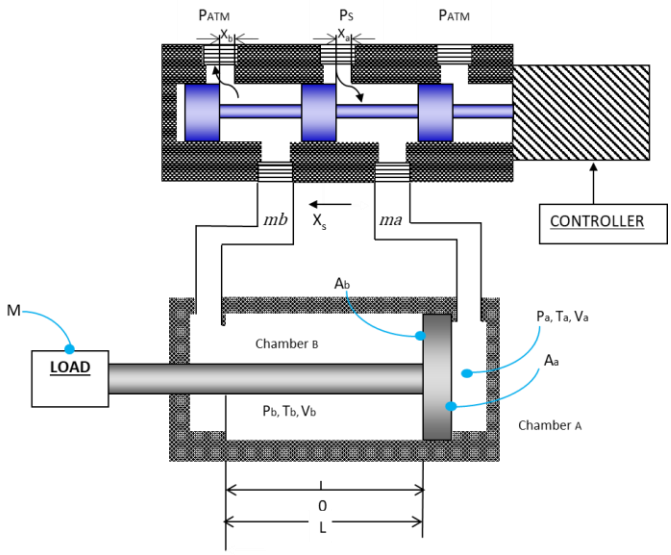

Figure 2: Servo-pneumatic systems.

The control valve inputs are the compressed air supply and spool displacement of the valve and the output is the compressed air flow to cylinder chambers.

$$\dot{m}_a = C_d C_o W_a X_a f(P_a, P_s, P_e) \quad (1)$$

$$\dot{m}_b = C_d C_o W_b X_b f(P_b, P_s, P_e) \quad (2)$$

Where C_d is the discharge coefficient, W is the port width of the valve, $X_{a,b}$ is the spool displacement of the valve, P_s is the supply pressure, P_e is the exhaust pressure, P_a is the chamber A pressure, P_b is the chamber B pressure.

$$f(P_a, P_s, P_e) = \frac{P_s f(P_a/P_s)}{\sqrt{T_s}}, chamber\ A\ is\ a\ drive\ chamber \quad (3)$$

$$f(P_b, P_s, P_e) = \frac{P_b f(P_e/P_b)}{\sqrt{T_b}}, chamber\ A\ is\ a\ drive\ chamber \quad (4)$$

$$f(P_a, P_s, P_e) = \frac{P_a f(P_e/P_a)}{\sqrt{T_a}}, chamber\ B\ is\ a\ drive\ chamber \quad (5)$$

$$f(P_b, P_s, P_e) = \frac{P_s f(P_b/P_s)}{\sqrt{T_s}}, chamber\ B\ is\ a\ drive\ chamber \quad (6)$$

And

$$f(P_r) = \begin{cases} 1, & P_{atm}/P_u < P_r < C_r \\ C_k\left[P_r^{2/K} - P_r^{(K+1)/K}\right]^{1/2}, & C_r < P_r < 1 \end{cases} \quad (7)$$

Where T_s is the supply temperature, T_a is the temperature of chamber A, T_b is the temperature of chamber B and $P_r = P_d/P_u$ is the ratio between the downstream pressure and upstream pressure through the orifice.

The specific heat ratio of the air K is used to calculate the critical pressure.

$$C_r = \left(\frac{P_d}{P_u}\right)_{CRIT} = \left(\frac{2}{K+1}\right)^{\frac{K}{K-1}} \quad (8)$$

The relationship between the cylinder inlet and outlet pressures and mass flow rates can be calculated by the following equations.

$$\dot{P}_a = \frac{K}{(L/2 + x + \Delta)}\left[-P_a\dot{x} + \frac{RT_s}{A_a}\dot{m}_a\right] \quad (9)$$

And

$$\dot{P}_b = \frac{K}{(L/2 - x + \Delta)}\left[P_b\dot{x} - \frac{RT_s}{A_b}\dot{m}_b\right] \quad (10)$$

Where x is the piston position, L is the stroke length, $-L/2 \leq x \leq L/2$, Δ is the equivalent residual length of the pneumatic cylinder generated by the connecting tube and components, R is the universal gas constant, A is the ram area.

The relationship between the pressure difference and the motion of the piston is given by:

$$\dot{v} = \frac{1}{M}[A_a P_a - A_b P_b - K_f v - F_r(x)] \quad (11)$$

Where v is the velocity, $\dot{v}$ is the acceleration, M is the payload mass, K_f is dynamic friction coefficient, $F_r(x)$ is the position-dependent resistance force. The system parameters used in this study are listed in Table 1.

3. System identification

System definition is a mathematical tool and algorithm that builds dynamic models from measured input and output data. The algorithm of the system identification iterative process is shown in Figure 3.

3.1 ARMA model and recursive estimation algorithm

ARMAX model structure is defined as follows:

$$X(t) + a_1X(t-1) + \cdots + a_{n_a}X(t-n_a) = b_1X_s(t-n_k) + \cdots + b_{n_b}X_s(t-n_k-n_b+1) + e(t) + c_1e(t-1) +$$

$c_{n_c} e(t - n_c)$
(12)

Table 1: Illustrate system parameters.

S/N	Symbols	Value	Description	unit
1	P_s	6	Working supply pressure	N/m^2
2	P_e	1	Exhaust pressure	N/m^2
3	P_{ATM}	1×10^5	Atmospheric pressure	N/m^2
4	$X_{a,b}$	4×10^{-3}	Valve spool displacement	m
5	$W_{a,b}$	0.0062	Port width	m
6	T_s	293	Supply temperature	K
7	T_a	293	Chamber A temperature	K
8	T_b	293	Chamber B temperature	K
9	C_d	0.8	Discharge coefficient	-----
10	C_r	0.528	Flow constant	-----
11	C_k	3.864	Flow constant	-----
12	K	1.4	Ratio of specific heat	-----
13	R	287	Universal gas constant	$J/(kg.K)$
14	D	0.042	Cylinder diameter	m
15	d	0.016	Rod diameter	m
16	L	0.26	Stroke length	m
17	Δ	0	Residual length	m
18	K_f	78	Dynamic friction coefficient	Ns/m
19	$F_r(x)$	83	Static friction force	N
20	M	1.9	Payload mass	kg

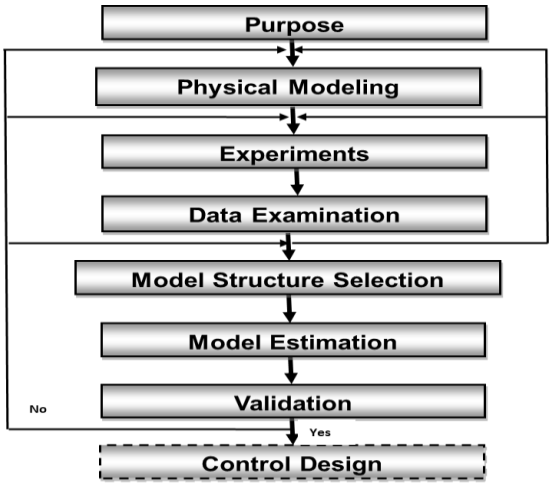

Figure 3: Algorithm for modeling and system identification.

Where $X(t)$ is the system output, $a_1 \dots a_n$, $b_1 \dots b_n$, $c_1 \dots c_n$ are the updated parameters, n_a is the system poles, $n_b - 1$ is the system zeros, n_c is the previous error terms, n_k is the number of input samples that occur before the inputs affecting the current output, $X(t-1) \dots X(t-n_a)$ are the previous outputs, $X_s(t-n_k) \dots X_s(t-n_k-n_b+1)$ are the previous inputs, $e(t)$, $e(t-1), e(t-n_c)$ White noise disturbance values.

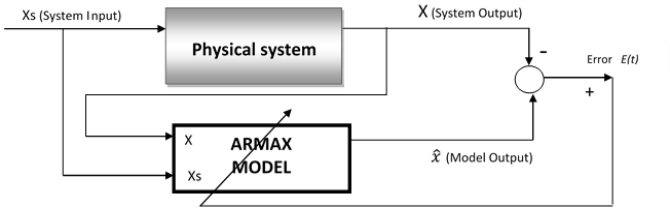

Figure 4: Auto-regressive moving-average (ARMAX) model.

The estimated system output $\hat{X}$ is a function of the previous outputs, current input, previous inputs, and model parameters. The objective is to detect a linear model that gives a predicted output $\hat{X}$ equal to the system output X. The least square error between the real output and the predicted output can be described by the following equation:

$$Error = E(t) = \frac{1}{2}\sum_{n=1}^{N}(\hat{X}(t) - X(t))^2 \quad (13)$$

where $E(t)$ is the prediction error, Xs is the system input, X is the system output. They are used to calculate the estimated output. Auto-regressive moving-average (ARMAX) model is shown in Figure 4.

4. Experimental test rig

The experimental test rig is integrated from mechanical and electronic components with a computer interface with high computational accuracy. The main components of the test rig are the proportional valve, double-acting cylinder, air service unit, potentiometer, rack and pinion, compressor, data acquisition card. The pneumatic system consists of a pneumatic power supply of 2.5 HP connected to the air service unit. The servo pneumatic valve was a 1/4-inch port, while the pneumatic actuator had a piston diameter of 42 mm, rod diameter of 16 mm, and the stroke length of 260 mm. The rack and pinion mechanism is attached to the piston of the cylinder, a rotary potentiometer of 5 kΩ is fixed on the pinion gear with a voltage source of 5 V, which is utilized to detect the piston motion. All input and output signals were sent and received with the computer via a National Instruments (NI) DAQ card with a sampling rate of 250 kS/s. A photograph of the test rig of the Pneumatic System is shown in Figure 5.

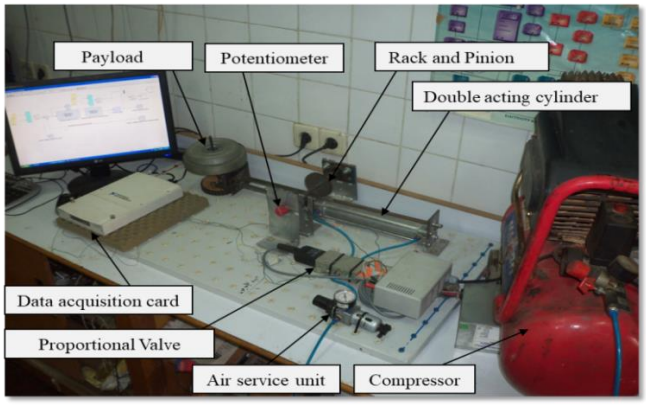

Figure 5: Photograph of the test rig of the pneumatic system.

5. Mixed-reality environment for the controller parameters identification

The mixed reality environment is usually based on the operation of the real system in conjunction with the simulation model as shown in Figure 6. The system identification method is used to acquire the system model accurately through the actual system inputs and outputs. Then, the offline optimization of the system controller will be performed on the system model to apply it to the real system.

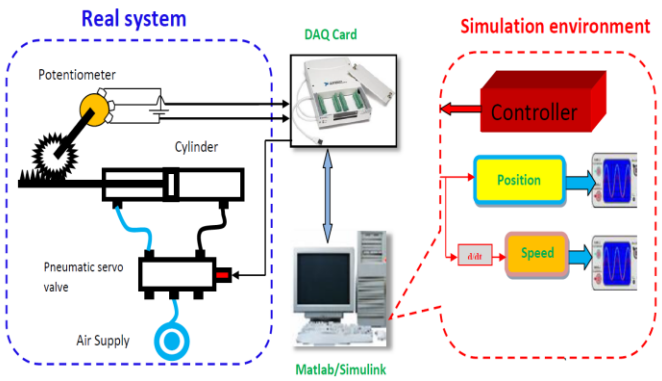

Figure 6: Mixed reality environment.

6. Experimental results

The online identification was performed on the real system by a set of experiments using the ARMA model under the impulse input signal. Figure 7 shows the Simulink model of the real system with ARMA model.

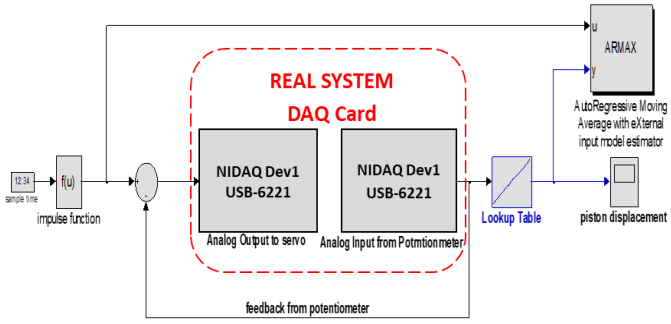

Figure 7: Simulink block diagram of the real system with ARMAX.

6.1 The effect of prediction orders on the system model

Several experiments were performed using third, fourth, and fifth orders to explain the effect of the model orders in the system model response. Figure 8 shows the comparison between the actual response and the third order response under one step prediction. The square error in the predicted model was $9.34e^{-6}$ cm and standard deviation of 0.001532 cm. therefore, the resulting transfer function is:

$$H(z) = \frac{1.557\,Z^{\wedge}2 + 0.4883\,Z + 0.020353}{Z^{\wedge}3 + 0.32635\,Z^{\wedge}2 + 0.055097\,Z + 0.01184}$$

Figure 9 shows the comparison between the actual response and fourth order response under one step prediction. The square error in the predicted model was $9.29e^{-6}$ cm and the standard deviation of 0.001527 cm. therefore, the resulting transfer function:

$$H(z) = \frac{1.5265\,Z^{\wedge}3 + 1.2318\,Z^{\wedge}2 + 1.1036\,Z - 0.0030112}{Z^{\wedge}4 + 0.82665\,Z^{\wedge}3 + 0.77581\,Z^{\wedge}2 + 0.041607\,Z + 0.027019}$$

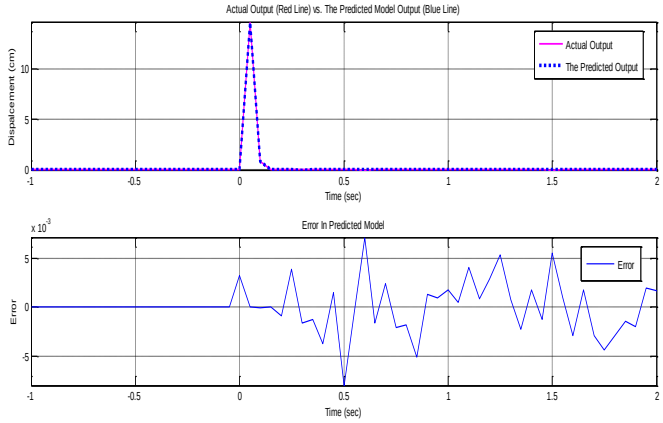

Figure 8: Comparison between the actual response and third order response under one step prediction.

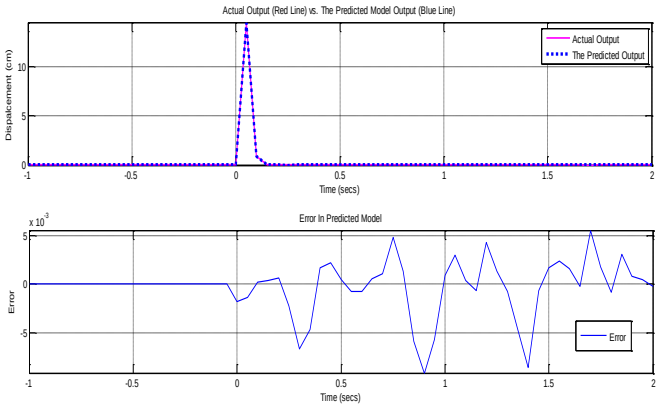

Figure 9: Comparison between the actual response and fourth order response under one step prediction.

Figure 10 shows the comparison between the actual response and fifth order response under one step prediction. The square error in the predicted model was $2.14e^{-5}$ cm and the standard deviation of 0.00232 cm. therefore, the resulting transfer function:

$$H(z) = \frac{1.5317\,Z^{\wedge}4 - 2.8807\,Z^{\wedge}3 + 1.4205\,Z^{\wedge}2 - 0.074304\,Z - 0.0049132}{Z^{\wedge}5 - 1.8633\,Z^{\wedge}4 + 0.93297\,Z^{\wedge}3 - 0.10507\,Z^{\wedge}2 + 0.032798\,Z - 0.00267}$$

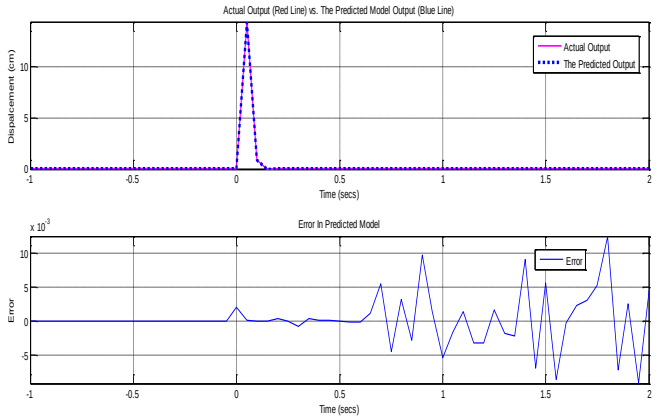

Figure 10: Comparison between the actual response and fifth order response under one step prediction.

The servo pneumatic system model was represented by four state variables according to the load dynamics equation 11. Therefore, it can be seen that the fourth-order system model achieved the best representation of the actual system with the least squared error.

6.2 The effect of the number of step predictions on the system model.

The experiments were performed using the fourth order model with different prediction step sizes. The effect of the number of step predictions was investigated using one, five, and ten steps. Figure 11 shows the comparison between the actual response and fourth order response under five step prediction. The square error in the predicted model was $3.31e^{-5}$ cm and the standard deviation of 0.001716 cm. therefore, the resulting transfer function:

$$H(z) = \frac{1.5222\,Z^3 - 1.1576\,Z^2 + 1.0276\,Z + 0.024444}{Z^4 - 0.74429\,Z^3 + 0.69887\,Z^2 - 0.00086195\,Z + 0.024871}$$

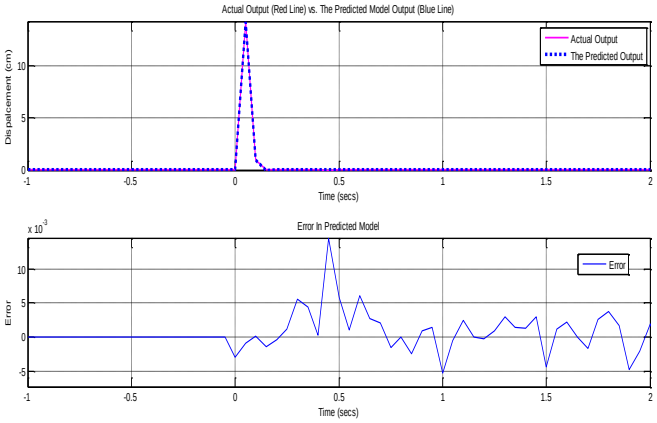

Figure 11: Comparison between the actual response and fourth order response under five step prediction.

Figure 12 shows the comparison between the actual response and fourth order response under ten step prediction. The square error in the predicted model was $3.31e^{-5}$ cm and the standard deviation of 0.002884 cm. therefore, the resulting transfer function:

$$H(Z) = \frac{1.5084\,Z^3 - 0.1845\,Z^2 - 0.98753\,Z - 0.043927}{Z^4 - 0.10416\,Z^3 - 0.62197\,Z^2 - 0.046606\,Z - 0.023213}$$

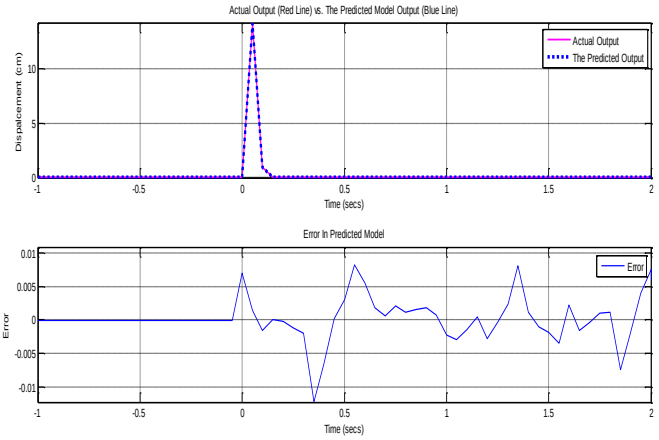

Figure 12: Comparison between the actual response and fourth order response under ten step prediction.

It can be seen that the minimum square error between the real system and the predicted model was with the one-step prediction model. There was a noticeable delay in tracking the response of the system with the five and ten step prediction models due to the nonlinearity of the system. Table 2 shows a comparison between the actual output and predicted model output with the different prediction orders. The result showed the fourth order ARMAX model under one step prediction was achieved the minimum square error. Therefore it was used for the offline PID controller adjustment.

Table 2: Comparison of the square error of different prediction orders under one step prediction.

Transfer function order	Signals	Statistical criteria			
		Minimum	Maximum	Square error	Standard deviation
Third order	Real output	-0.007084	14.64	$9.34e^{-06}$	1.037
	Predicted model	-0.004885	14.64		1.037
	Error	-0.007972	0.007137		0.001532
Fourth order	Real output	-0.005816	14.56	$9.29e^{-06}$	1.031
	Predicted model	0.005549	14.56		1.031
	Error	-0.009141	0.005538		0.001527
Fifth order	Real output	-0.01976	14.4	$2.14e^{-05}$	1.02
	Predicted model	-0.01974	14.4		1.02
	Error	-0.009149	0.01243		0.00232

Ziegler-Nicholas method is used for the tuning of the controller parameters, after several trial and error run, the controller gains are K_p=16, K_i=6, and K_d=0.001. The optimized PID controller was applied to the servo pneumatic system to investigate the system performance as shown in Figure13.

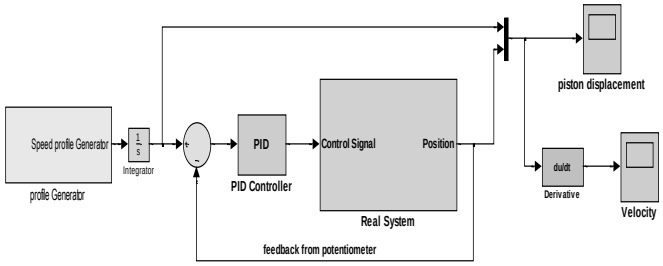

Figure 13: Real servo pneumatic system.

Figure 14 shows the comparison between the simulated, predicted model and real system position response due to step input 6 cm. It can be seen that the predicted model can track the actual output of the system with better accuracy than the simulation model. Figures 15 and 16 show the comparison between the simulated model position and real system position with different demand positions. The result showed that the predicted system model has a good match with the actual output response with minimum error.

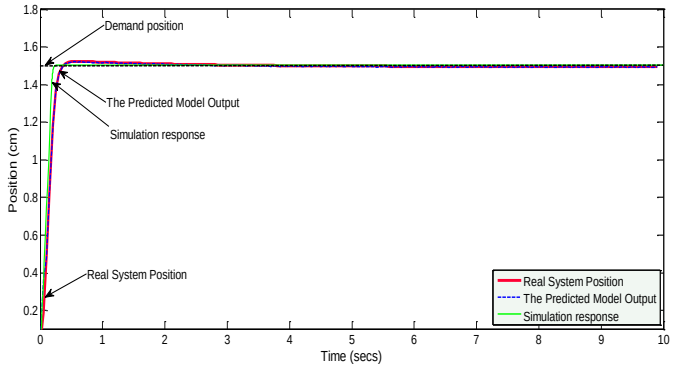

Figure 14: Comparison between the simulated, predicted model and real system position response due to step input.

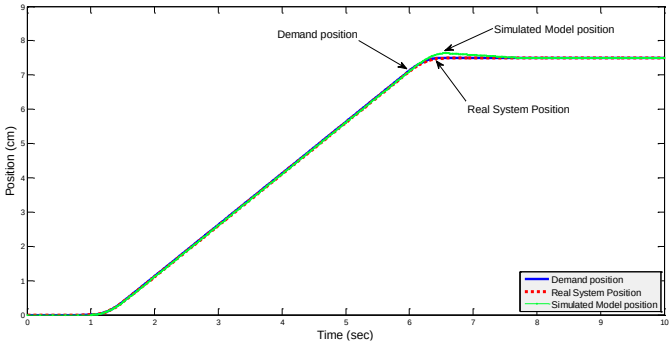

Figure 15: Comparison between the simulated model position and real system position with demand positions.

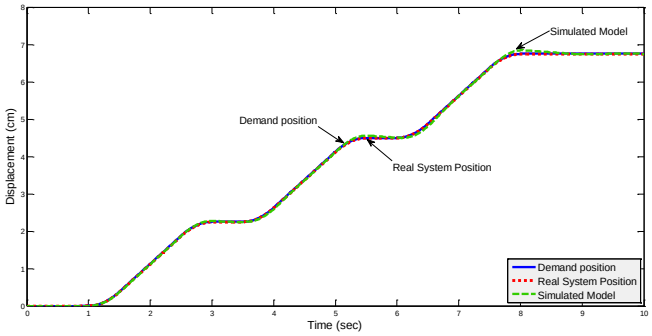

Figure 16: Comparison between simulated model position and real system position with multiple position profiles.

7. Conclusions

In this paper, a mixed reality environment is used to identify and control the servo pneumatic system. The auto-regressive moving-average (ARMA) model-based recursive least squares (RLS) algorithm was proposed and implemented in a real-time environment. Online identification was utilized efficiently using the suggested method. The results showed that the proposed method is an easy, accurate, and robust method to control and identify the servo pneumatic system. The experimental and simulation results showed a good matching with the demand different positions. Moreover, the suggested method used to control the servo pneumatic system showed good performance in tracking multiple position profiles.

References

[1] Moore, P., and Pu, J. S., "Pneumatic servo actuator technology," IEE Colloquium on Actuator Technology: Current Practice and New Developments, 1996. https://doi.org/10.1049/ic:19960694.

[2] Richard, E., and Scavarda, S., "Comparison between linear and nonlinear control of an electropneumatic servodrive," J Dyn Syst Meas Control, 1996(118): p. 245-252. https://doi.org/10.1115/1.2802310.

[3] Keller, H., and Isermann, R., "Model-based nonlinear adaptive control of a pneumatic actuator," Control Engineering Practice, 1993. **1**(3): p. 505-511. https://doi.org/10.1016/0967-0661(93)91888-4.

[4] Wang, J., Pu, J., and Moore, P., "A practical control strategy for servo-pneumatic actuator systems," Control Engineering Practice, 1999. **7**(12): p. 1483-1488. https://doi.org/10.1016/S0967-0661(99)00115-X.

[5] Wang, J., Pu, J., and Moore, P., "Accurate position control of servo pneumatic actuator systems: an application to food packaging," Control Engineering Practice, 1999. **7**(6): p. 699-706.

[6] Jalal, S. S., and Batur, C. "Sliding mode motion control of a pneumatic cylinder." in ASME International Mechanical Engineering Congress and Exposition. 2004.

[7] Ning, S., and Bone, G. M. "High steady-state accuracy pneumatic servo positioning system with PVA/PV control and friction compensation." in Proceedings 2002 IEEE international conference on robotics and automation (Cat. No. 02CH37292). 2002. IEEE.

[8] Wang, J., Pu, J., Moore, P. R., and Zhang, Z., "Modelling study and servo-control of air motor systems," International Journal of Control, 1998. **71**(3): p. 459-476.

[9] Lai, W., Rahmat, M., and Wahab, N. A., "MODELING AND CONTROLLER DESIGN OF PNEUMATIC ACTUATOR SYSTEM WITH CONTROL VALVE," International Journal on Smart Sensing & Intelligent Systems, 2012. **5**(3).

[10] Syed Salim, S. N., Rahmat, M. F. a., Mohd Faudzi, A. A., Ismail, Z. H., and Sunar, N., "Position Control of Pneumatic Actuator Using Self-Regulation Nonlinear PID," Mathematical Problems in Engineering, 2014. **2014**: p. 1-12. https://doi.org/10.1155/2014/957041.

[11] Ren, H.-P., Fan, J.-T., and Kaynak, O., "Optimal Design of a Fractional-Order Proportional-Integer-Differential Controller for a Pneumatic Position Servo System," IEEE Transactions on Industrial Electronics, 2019. **66**(8): p. 6220-6229. https://doi.org/10.1109/tie.2018.2870412.

[12] Awad, M., Sokar, M. I., Abdrabbo, S. M., and El-Arabi, M., "Hydro-Pneumatic Energy Harvesting Suspension System Using a PSO Based PID Controller," SAE Int. J. Commer. Veh., 2018. **11**(4): p. 223-234. https://doi.org/10.4271/02-11-04-0018.

[13] Azahar, M. I. P., Irawan, A., and Taufika, R. M., "Fuzzy Self-Adaptive PID for Pneumatic Piston Rod Motion Control," 2019: p. 82-87. https://doi.org/10.1109/icsgrc.2019.8837064.

[14] Irawan, A., and Azahar, M. I. P., "Cascade Control Strategy on Servo Pneumatic System with Fuzzy Self-Adaptive System," Journal of Control, Automation and Electrical Systems, 2020. **31**(6): p. 1412-1425. https://doi.org/10.1007/s40313-020-00642-4.

[15] Awad, M. N., Sokar, M. I., Rabbo, S. A., and El-Arabi, M., "Performance evaluation and damping characteristics of hydro-pneumatic regenerative suspension system," International Journal of Applied Engineering Research, 2018. **13**(7): p. 5436-5442.

[16] dos Santos, M. P. S., and Ferreira, J., "Novel intelligent real-time position tracking system using FPGA and fuzzy logic," ISA transactions, 2014. **53**(2): p. 402-414.

[17] Najjari, B., Barakati, S. M., Mohammadi, A., Futohi, M. J., and Bostanian, M., "Position control of an electro-pneumatic system based on PWM technique and FLC," ISA transactions, 2014. **53**(2): p. 647-657.

[18] Kamaludin, K. N., Abdullah, L., Salim, S. N. S., Jamaludin, Z., and Maslan, M. N., "Improvement of a Proportional-Integral (PI) Controller for a Servo Pneumatic Actuator by Adapting Zero-Compensator Placement Method," 2021: p. 222-226. https://doi.org/10.1109/icsgrc53186.2021.9515278.